The Company of **Biologists**

RESEARCH ARTICLE

Real-time 3D visualization of cellular rearrangements during cardiac valve formation

Jenny Pestel[1], Radhan Ramadass[1], Sebastien Gauvrit[1], Christian Helker[1,2], Wiebke Herzog[2,3] and Didier Y. R. Stainier[1],*

ABSTRACT

During cardiac valve development, the single-layered endocardial sheet at the atrioventricular canal (AVC) is remodeled into multilayered immature valve leaflets. Most of our knowledge about this process comes from examining fixed samples that do not allow a real-time appreciation of the intricacies of valve formation. Here, we exploit non-invasive *in vivo* imaging techniques to identify the dynamic cell behaviors that lead to the formation of the immature valve leaflets. We find that in zebrafish, the valve leaflets consist of two sets of endocardial cells at the luminal and abluminal side, which we refer to as luminal cells (LCs) and abluminal cells (ALCs), respectively. By analyzing cellular rearrangements during valve formation, we observed that the LCs and ALCs originate from the atrium and ventricle, respectively. Furthermore, we utilized Wnt/β-catenin and Notch signaling reporter lines to distinguish between the LCs and ALCs, and also found that cardiac contractility and/or blood flow is necessary for the endocardial expression of these signaling reporters. Thus, our 3D analyses of cardiac valve formation in zebrafish provide fundamental insights into the cellular rearrangements underlying this process.

KEY WORDS: Cardiac valves, Endocardium, Live imaging, Notch, Wnt, Zebrafish, Apc

INTRODUCTION

The correct formation and function of cardiac valves is crucial to ensure efficient blood pumping of the heart. Malformation of the cardiac valves can lead to severe deterioration of the heart and is also the leading cause of birth-related deaths (Lloyd-Jones et al., 2010). Furthermore, minor abnormalities of cardiac valves often remain undetected until they cause severe problems later in life. Despite the widespread occurrence of heart valve defects, a fundamental understanding of the cellular processes leading to the formation of heart valves is still lacking.

During development, the formation of cardiac valves becomes necessary to prevent retrograde blood flow. The primitive embryonic heart in zebrafish is a linear tube that has been reported to function as a suction pump (Forouhar et al., 2006), which efficiently pumps blood from the atrium to the ventricle. However, after the heart tube has undergone complex morphogenetic movements resulting in a looped organ, the blood pumping performance of the heart decreases

(Liebling et al., 2006); therefore, cardiac valves are needed. Formation of cardiac valves takes place at the junction of the atrium and ventricle – the atrioventricular canal (AVC). At the beginning of valve formation, endocardial cells at the AVC migrate into a wide extracellular matrix called the cardiac jelly. Here, they proliferate to form endocardial cushions. These endocardial cushions will later remodel to form the mature valve leaflets. The formation of cardiac valves is orchestrated by a number of signaling pathways (Armstrong and Bischoff, 2004), including Notch (Timmerman et al., 2004), ErbB (Camenisch et al., 2002; Iwamoto et al., 2003), Bmp (Kim et al., 2001; Ma et al., 2005; Rivera-Feliciano et al., 2006), TGF-β (Brown et al., 1999), Wnt (Gitler et al., 2003; Hurlstone et al., 2003) and NFAT (de la Pompa et al., 1998; Ranger et al., 1998). There is strong evidence that these signaling pathways interact with each other to regulate cardiac valve formation (Armstrong and Bischoff, 2004; Timmerman et al., 2004; Ahuja et al., 2016). Although signaling during cardiac valve formation has been extensively studied, the precise role of the different pathways in modulating individual cell behavior is largely unknown.

One of the main challenges in studying organogenesis of the heart, and in particular the formation of cardiac valves, is the strong interdependence between genetic and environmental factors. For example, modifications of intracardiac flow due to cardiac shape or contractility changes, lead to disturbances in heart development and maturation (Bartman et al., 2004; Auman et al., 2007). Any conformational changes are likely to affect intracardiac flow patterns and, thus, valve formation. Indeed, embryos with disturbed intracardiac hemodynamics exhibit valve defects (Auman et al., 2007; Vermot et al., 2009; Kalogirou et al., 2014). However, the role of different signaling molecules involved in valve formation has mainly been studied in explants or fixed tissue samples, where the influence of environmental factors on genetic factors and vice versa cannot be investigated. Therefore, a model system where the genetic factors underlying cardiac valve formation are conserved and which allows visualization of this process *in vivo*, is crucial for a complete understanding of the development of cardiac valves. Transparent zebrafish embryos, which allow high-resolution live cell imaging, fulfil these criteria (Beis and Stainier, 2006). Additionally, the zebrafish model offers several distinct attributes, including external fertilization, rapid development and the ability to survive severe heart defects for several days (Stainier, 2001). In the two-chambered zebrafish heart, cardiac valve formation starts at 55 hours post-fertilization (hpf) as squamous endocardial cells at the AVC differentiate and adopt a cuboidal shape. Later, at 60 hpf, endocardial cells start to invade the cardiac jelly (Beis et al., 2005). Although signaling pathways regulating cardiac valve formation, such as ErbB (Goishi et al., 2003), NFAT (Chang et al., 2004), TGF-β (Scherz et al., 2008) and Notch (Timmerman et al., 2004) are conserved, it has been reported that

[1]Max Planck Institute for Heart and Lung Research, Department of Developmental Genetics, Bad Nauheim 61231, Germany. [2]University of Muenster, Muenster 48149, Germany. [3]Cells-in-Motion Cluster of Excellence (EXC 1003 - CiM), University of Muenster, Muenster 48149, Germany.

*Author for correspondence (didier.stainier@mpi-bn.mpg.de)

D.Y.R.S., 0000-0002-0382-0026

DEVELOPMENT

instead of forming mesenchymal endocardial cushions, the zebrafish heart displays an immature valve, which is later remodeled into mature valve leaflets (Beis et al., 2005). The immature valve seems to be formed by invagination of the endocardial AVC layer (Scherz et al., 2008) and is clearly detectable by 72 hpf (Beis et al., 2005). This observation that the zebrafish cardiac valves seem to form by invagination could only be made by high-speed imaging, which illustrates the importance of analyzing valve development *in vivo* (Scherz et al., 2008). Nonetheless, the detailed anatomy of immature valves in zebrafish embryos is largely unknown. Such knowledge is, however, crucial to study how signaling molecules involved in cardiac valve formation modulate endocardial cell behavior.

Here, we use an imaging approach that takes the complexity of the heart into account and allows for 3D rendering of the cellular rearrangements underlying valve formation in live embryos. We describe the progressive transformation from the single-layered endocardium overlying the AVC into multilayered immature valves and track the behavior of individual cells during this process. We find that the immature valve is organized into two molecularly distinct structures. Furthermore, by using Wnt/β-catenin and Notch reporter fish, we monitor the activity of these key signaling pathways during valve formation at single-cell resolution and also analyze the influence of cardiac contraction on these pathways. Finally, we re-examine the valve phenotype in *apc* mutants and find that Wnt/β-catenin signaling regulates multiple processes that impact cardiac valve formation.

RESULTS

### The immature valve comprises two different sets of cells

In order to shed light onto the cellular rearrangements underlying valve formation in zebrafish, we first analyzed the detailed organization of the immature valve at single-cell resolution in 3D in living embryos and larvae. For this study, we mated

Tg(kdrl:gfp) zebrafish, expressing cytosolic EGFP in endothelial cells (Jin et al., 2005) with the Wnt/β-catenin reporter fish *Tg(7xTCF-Xla.Siam:nls-mCherry)*, which expresses a red nuclear fluorophore. As Wnt/β-catenin signaling has been reported to be active during valve formation (Gitler et al., 2003; Hurlstone et al., 2003; Moro et al., 2012), the Wnt/β-catenin reporter line provides an excellent tool to monitor cellular reorganizations within the valve-forming area. We began our analyses at 75 hpf, after obvious structures of the immature valve have been formed (Beis et al., 2005). The coexpression of EGFP and mCherry highlights the forming valvular structures at the inner and outer ventricular curvatures (Fig. 1A-A″), which are referred to as superior and inferior forming valve leaflets, respectively. Since the leaflet of the superior AVC develops first, we focused our studies on this leaflet. To understand the compositional organization of the immature valve leaflet at cellular resolution, we 3D volume rendered the acquired *z*-stack shown in Fig. 1A-A″ (Fig. 1B). To enhance the clarity of the endocardial AVC cells, we removed the nuclear *TCF*:mCherry signal, which did not overlap with endocardial EGFP during image processing. The volume-rendered heart was then used to study the 3D organization of the forming leaflet. We defined the sagittal, coronal and transverse planes based on the orientation of the linear heart tube at 28 hpf (Fig. 1B). These three planes were subsequently used as references to ensure that 3D datasets were always analyzed from the same perspective.

Examination of the 3D volume-rendered views in sagittal, coronal and transverse projections revealed that the immature valve leaflet is composed of two different cell layers: (1) a single cell layer lining the AVC, which we refer to as luminal cells (LCs) (Fig. 1C-E and red cells, Fig. 1C′-E′) and (2) a layer of cells sitting on top of this first layer and comprising the abluminal side of the immature valve, which we refer to as abluminal cells (ALCs) (Fig. 1C-E and Fig. 1C′-E′, blue cells).
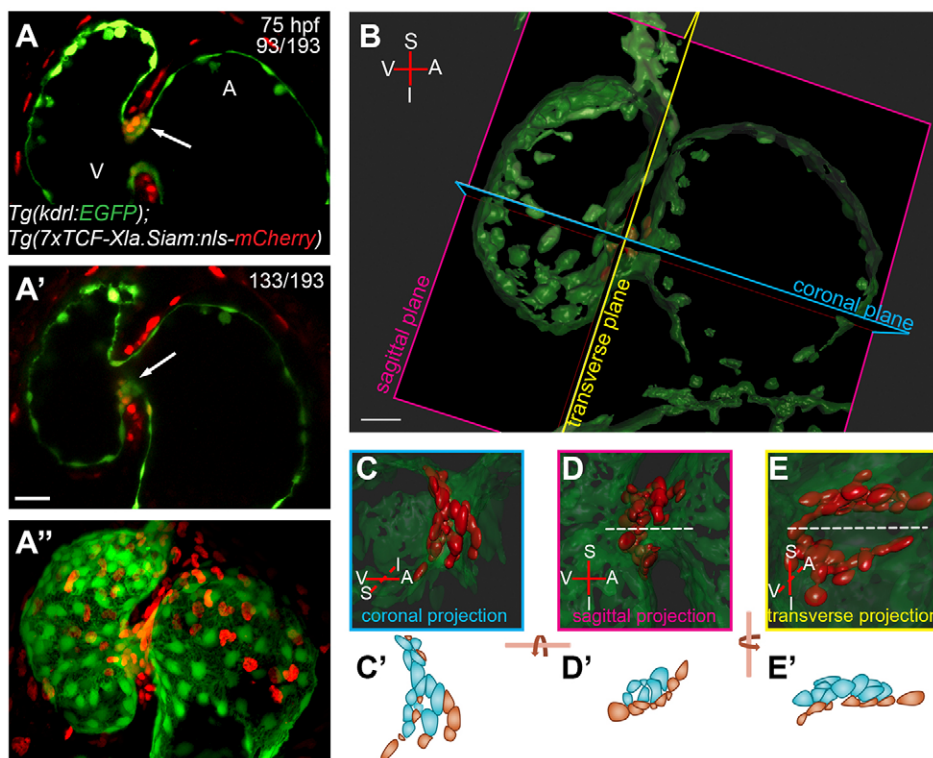
Fig. 1. 3D analysis of cardiac valve formation. (A-A″) *z*-stack of a 75 hpf *Tg(kdrl: EGFP);Tg(7xTCF-Xla.Siam:nls-mcherry)* heart; ventral view. Coexpression of endothelial-specific EGFP and *TCF*-driven mCherry marks the valve-forming cells in the single-plane images. Coexpression marking the superior part of the AVC is shown in *z*-stack plane 93 (A, arrow) and colocalization marking the inferior part of the AVC is shown in *z*-stack plane 133 (A′, arrow). Maximum projection of the *z*-stack is shown in A″. (B) 3D volume rendering of dataset from A. Note that Imaris software was used to remove the mCherry signal not co-occurring or overlapping with EGFP, so that only endocardial mCherry^{+} cells are shown. The coronal, sagittal and transverse planes of the heart were defined based on the orientation of the linear heart tube. (C-E) Close ups of the 3D volume rendered views in coronal, sagittal and transverse projections, respectively. The superior immature valve is above the dashed line in D and E. (C′,D′,E′) Cartoons of *TCF*: mCherry^{+} endocardial cells of the superior half of the AVC. Cells colored in blue represent abluminal cells (ALCs) and cells colored in reddish brown represent luminal cells (LCs). A, atrium; I, inferior AVC; S, superior AVC; V, ventricle. Scale bar: 20 μm.
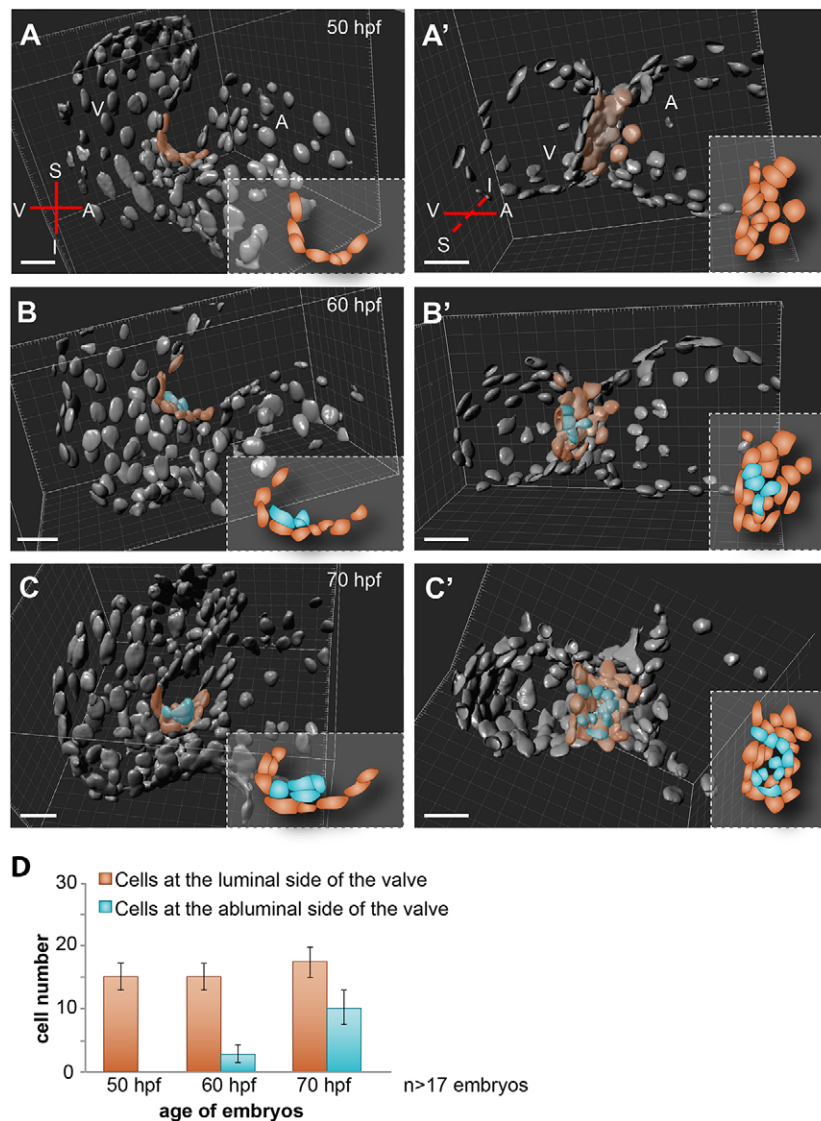
Fig. 2. Complex cell rearrangements form the immature valve leaflets. 3D volume renderings of *Tg(kdrl:nls-EGFP)* embryonic hearts of three representative examples at 50 (A,A′), 60 (B,B′) and 70 (C,C′) hpf. 3D volume rendered views in sagittal and coronal projections are shown in A-C and A′-C′, respectively. The single-layered AVC endocardium is remodeled into a multilayered structure by an increasing number of endocardial cells located at the abluminal side of the immature valve (false colored in blue). At 60 hpf, 4 (B,B′,D) and at 70 hpf, 10 (C,C′,D) cells are detected at the abluminal side of the valve. Quantification of the mean (±s.d.) number of cells at the luminal and abluminal sides of the forming valve is shown in D. At 50 hpf, cells at the superior AVC were counted in 19 embryos, at 60 hpf in 17 embryos and at 70 hpf in 20 embryos. Blue cells represent those located at the abluminal side and reddish brown cells represent those at the luminal side of the forming valve. Cartoons depict cell arrangements observed at the superior AVC. A, atrium; I, inferior AVC; S, superior AVC; V, ventricle. Scale bars: 20 μm.

Atrial and ventricular endocardial cells contribute to the formation of the immature valve

To investigate the cellular rearrangements underlying the transformation from the single-layered AVC endocardial sheet into multi-layered immature valves, we visualized the spatial organization of the emerging valve leaflet over time. For this purpose, we employed *Tg(kdrl:nls-GFP)* embryos, which express nuclear GFP in endocardial cells, and acquired *z*-stacks of the hearts at 50, 60 and 70 hpf. Subsequently, we 3D volume rendered the *z*-stacks and analyzed the hearts in sagittal (Fig. 2A-C) and coronal (Fig. 2A′-C′) projections. At 50 hpf, we found evenly distributed cells lining the superior AVC (*n*=19 embryos) (Fig. 2A,A′). At 60 hpf, in addition to the lumen-lining cells observable at 50 hpf, we found an extra layer of cells on top of the LCs, which was composed of 3±1 ALCs (*n*=17 embryos) on average (Fig. 2B,B′,D). In all the hearts analyzed, the position of these early valvular structures was identical: the first cells breaking out of the lumen-lining layer were situated on top of the superior AVC, at the junction between the AVC and the inner ventricular curvature. Ten hours later, at 70 hpf, we detected additional cells (10±3 cells; *n*=20 embryos) on top of the LCs (Fig. 2C,C′,D). It has previously been reported that the immature valve leaflet has an S-shaped organization in 2D (Beis

et al., 2005). To identify the cellular structures from our 3D datasets that form the S-shaped valve leaflet, we analyzed sagittal, coronal and transverse planes of the hearts shown in Fig. 2. We found that the ALCs form the upper curves of the S-shaped leaflet and the LCs form its lower curve (Fig. S1).

In the next step, we examined whether ALCs needed to migrate over a long distance or whether they just ingressed from the underlying endocardium in order to form the abluminal side of the immature valve leaflet. Therefore, we used the *nfatc1* promoter to generate a transgenic line, *TgBAC(nfatc1:GAL4ff)*, which allows strong Kaede expression at the AVC at 55 hpf in *TgBAC(nfatc1:GAL4ff);Tg(UAS:Kaede)* embryos. To track endocardial cells over time, we photoconverted the Kaede protein at 55 hpf (Fig. 3A,A′). At 75 hpf, in addition to the photoconverted red fluorescent cells, we could detect green non-photoconverted fluorescent cells at the AVC (*n*=6 embryos) (Fig. 3B,B′). Since all AVC cells expressed Kaede at 55 hpf and all of these cells were successfully photoconverted, the detection of these new green fluorescent cells provides evidence for a contribution of endocardial cells from the atrial or ventricular chamber to the forming valve leaflet. However, cells at the abluminal side of the valve exhibited exclusively yellow to red fluorescence, suggesting that those ALCs originate from
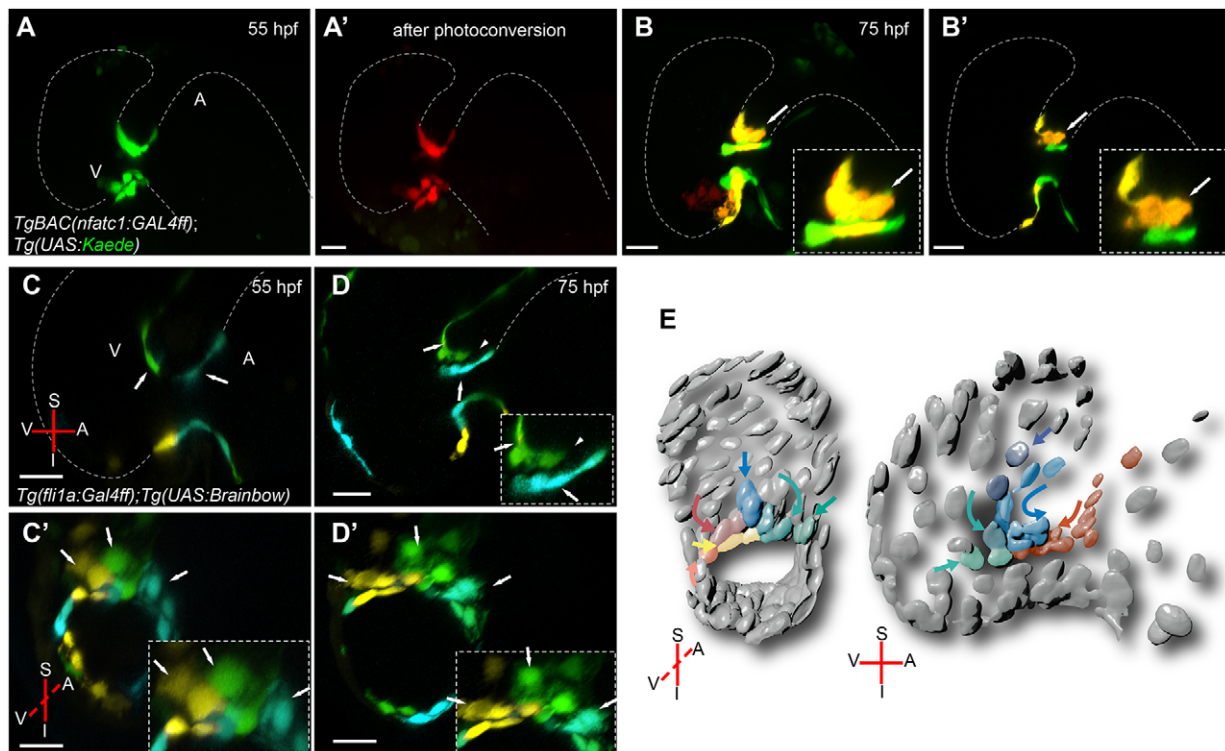
Fig. 3. Endocardial cell movements from the atrium and ventricle contribute to cardiac valve formation. 3D sagittal projection of a *TgBAC(nfatc1:GAL4ff); Tg(UAS:Kaede)* heart before (A) and after (A′) photoconversion at 55 hpf. Strong 'nfatc1' expression can be detected at the AVC. 3D projection (B) and optical section (B′) of the heart shown in A at 75 hpf. Arrows in B and B′ indicate forming valve. New green cells can be observed at the AVC indicating a contribution of *nfact1*-positive cells from outside the AVC to the valve region. Red fluorescent cells remain at the AVC. Magnifications of the forming valve are shown in B and B′, insets. (C,D) Sagittal planes of a *Tg(fli1a:Gal4ff);Tg(UAS:Brainbow)* heart. Embryos were injected with *Cre* mRNA at the one-cell stage and imaged at 55 (C) and 75 (D) hpf. Green fluorescent cells located in the ventricle at 55 hpf (C, green, arrow) appear to move towards the AVC (D). A subset of these cells can be detected in the abluminal side of the valve (D, arrowhead). Cyan fluorescent cells in the atrium also appear to move towards the AVC (D). However, these cells appear to join the group of cells lining the AVC lumen (D, cyan, arrow). (C′,D′) Transverse planes of the same datasets as in C and D, respectively. (E) A model of the deduced cell movements. A, atrium; I, inferior AVC; S, superior AVC; V, ventricle. Scale bars, 20 μm.

the single-layered AVC-endocardium observable at 55 hpf. Furthermore, we observed endocardial cells in the ventricle forming long protrusions towards the AVC in hearts of *Tg(Tp1: LifeAct-mCherry)* embryos, which express an F-actin marker in ventricular and AVC endocardium (Fig. S2), indicating that cell migration is involved during cardiac valve formation.

Based on the data from our photoconversion experiments, we conclude that atrial and ventricular endocardial cells contribute to the forming valvular structures. To track the movements of individual cells during cardiac valve formation, we analyzed mosaically labeled endocardial cells. For this purpose, we mated *Tg(fli1a:Gal4ff);Tg(UAS:Brainbow)* fish, which express a vascular-specific brainbow construct and injected *Cre* mRNA into one-cell stage embryos. The injection of *Cre* mRNA triggers a recombination event that leads to the random expression and combination of different fluorophores. Using this method, we were able to observe the movement of differently colored individual endocardial cells. Between 55 and 75 hpf, we observed endocardial cells in the ventricle moving towards the AVC and the abluminal side of the valve (Fig. 3C-E). However, endocardial cells in the atrium, which were also observed to move towards the AVC, never appeared to contribute to the abluminal population of the immature valve leaflet. Instead, these cells contributed to the luminal valvular structures (Fig. 3C-E). By examining transverse planes of the brainbow fluorescent hearts, we found that cells surrounding the AVC did not undergo dramatic changes in their position between 55

and 75 hpf. These cells appeared to remain at their location and assemble in a more organized manner (Fig. 3C,D′). In total, we examined 13 animals mosaically expressing fluorophores in their endocardial cells and from these observations created a model showing the deduced cell movements (Fig. 3E).

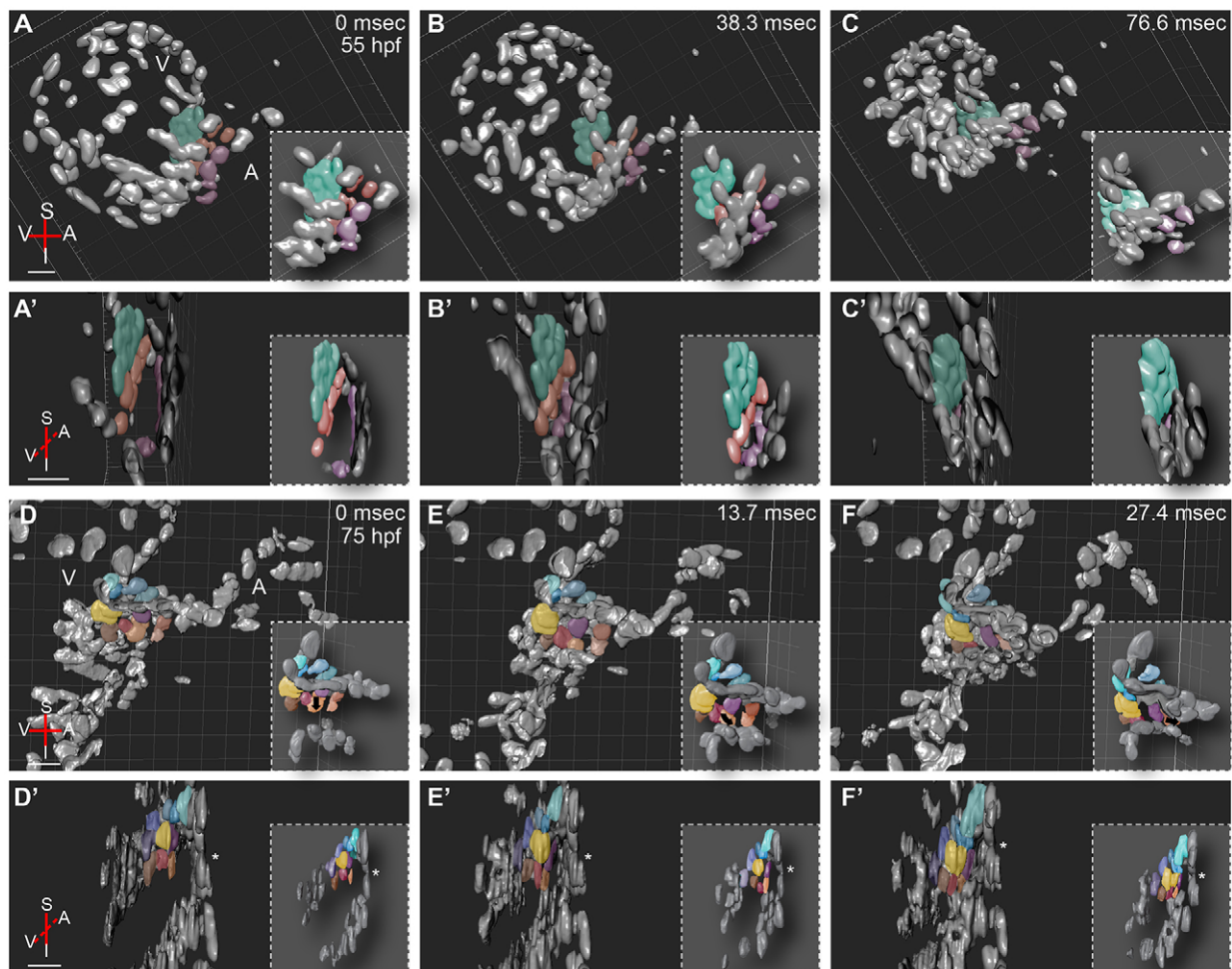### Cells at the abluminal side of the immature valve allow more efficient closure of the AVC

To understand how ALCs and LCs are associated and to examine how the growing number of these cells helps to prevent the retrograde blood flow, we analyzed the movement pattern of the immature valve leaflet during cardiac contraction. For this purpose, we acquired movies of the beating hearts of *Tg(kdrl:nls-egfp)* embryos and larvae with a spinning disk microscope at 55 and 75 hpf. For movie acquisition and processing, we took advantage of a previously published imaging approach allowing for 4D image reconstruction of fast-moving tissues (Liebling et al., 2005, 2006; Ohn et al., 2009). In brief, we recorded a movie of a single optical section for a few cardiac contraction cycles. After this movie was finished, we recorded the next optical section. This cycle was repeated until movies of all optical sections through the heart were collected. However, the movies of each single plane were triggered regardless of progression through the cardiac contraction cycle. Thus, the acquired movies had to be synchronized and post-processed using a previously published algorithm (Liebling et al., 2005, 2006; Ohn et al., 2009). Afterwards, the aligned movies of the

beating hearts were 3D volume rendered and the movement pattern of the immature valve analyzed. Examining the 3D rendered views in sagittal projections at 55 hpf, we found that the AVC contracts in a wave-like pattern during ventricular systole beginning from the atrium and moving towards the ventricle as reported from time-lapse movies of single confocal planes (Scherz et al., 2008) (Fig. 4A-C and Movie 1). When analyzing our dataset looking at transverse projections from the ventricle, we observed that the closure of the AVC starts at its atrial side. At 55 hpf, closure of the AVC is achieved by a ring of endocardial cells that progressively constricts (Fig. 4A′-C′ and Movie 2). Within 77.6 ms of the onset of constriction, the cells of the superior AVC also contributed to the closure of the AVC (Fig. 4C,C′), marking the most efficient point of AVC closure (Fig. 4C,C′). At 75 hpf, we observed an efficient closure of the AVC at 27.4 ms after the onset of constriction. At this stage, occlusion of the AVC also starts from the atrium during ventricular systole, but due to the increased number of ALCs, more cells and thus, a thicker layer of tissue is provided at the AVC. In this way, the growing number of ALCs helps to push the lumen-lining

cells to touch the opposite site of the AVC, thereby allowing for effective closure of the AVC (Fig. 4D-F′ and Movies 3 and 4).
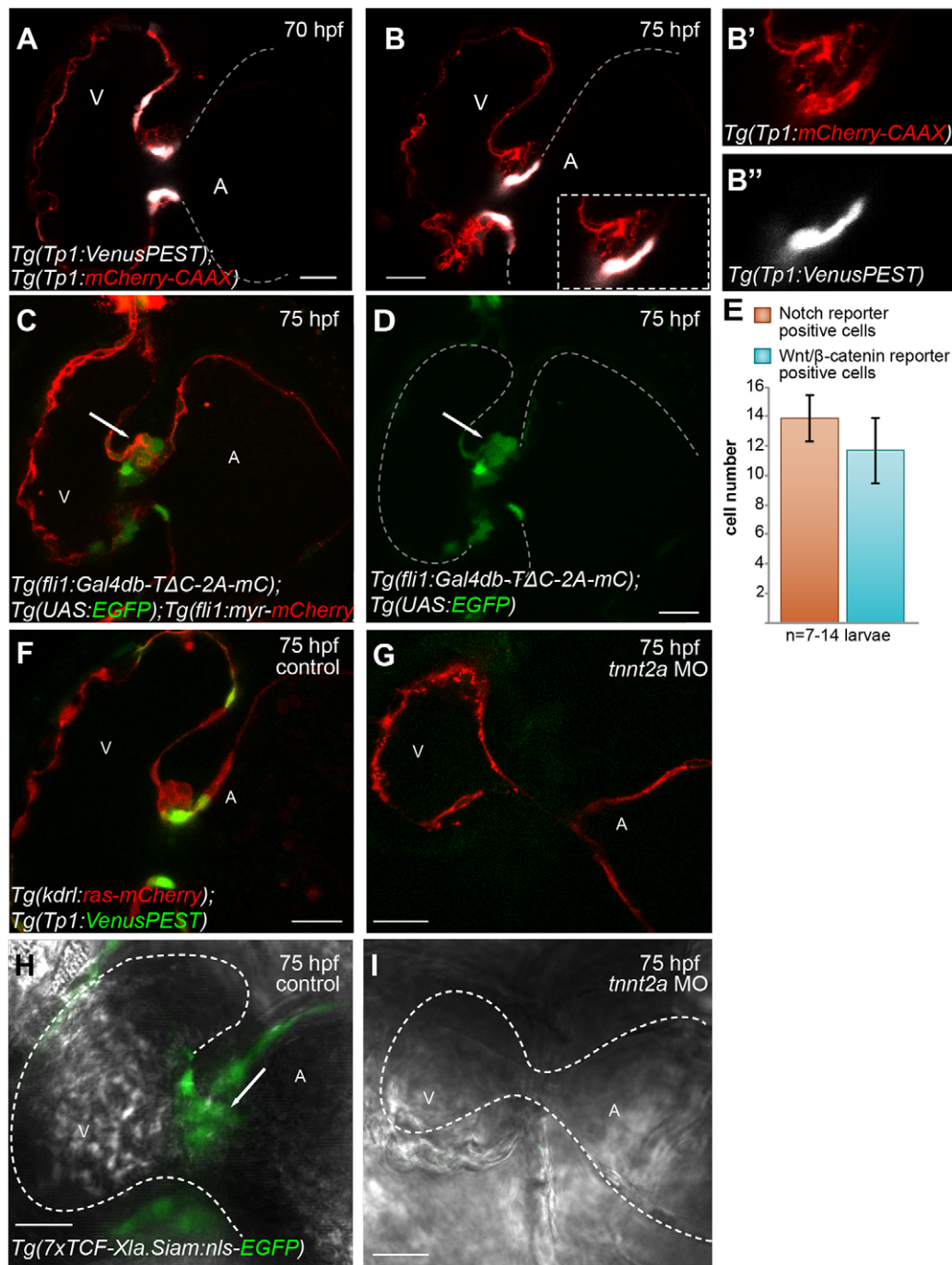
Notch and Wnt/β-catenin signaling reporters are primarily expressed in the luminal and abluminal cells, respectively

Based on our previous observation that ALCs are more motile than LCs, we investigated whether the differences between these cells were not only represented by different cellular behaviors, but also by different cell signaling activities. We focused our initial studies on Notch signaling. Mouse embryos defective for RBPJκ function exhibit atrophic valves and an abnormal upregulation of the intercellular adhesion molecule VE-cadherin (Timmerman et al., 2004), suggesting that Notch signaling is required to downregulate intercellular adhesions and to facilitate cell migration into the cardiac jelly. To investigate Notch activity at cellular resolution, we mated *Tg(Tp1:VenusPEST)* with *Tg(Tp1:mcherry-CAAX)* fish, in which the expression of both VenusPEST and mCherry-CAAX is driven by the Notch-responsive element *Tp1*. The fusion of the PEST domain to Venus destabilizes the fluorescent protein, thereby

Fig. 4. 4D analyses of beating hearts show that cells located at the abluminal side of the immature valve contribute to a more efficient closure of the AVC. 3D volume rendering of a *Tg(kdrl:nls-EGFP)* heart in different contraction stages in sagittal (A-F) and transverse (A′-F′) projections. Unsynchronized z-stacks of a beating heart were taken at 55 and 75 hpf. The images were post-acquisitionally aligned. For a better understanding of the cell movements during cardiac contraction, a subset of cells was false colored. At 55 hpf, cells at the atrial side of the AVC (purple and red) form a ring that progressively constricts to achieve the closure of the AVC (A′,B′). During ventricular systole, cells lining the ventricular side of the AVC (false colored in green) also support the closure of the AVC. At 75 hpf, the closure of the AVC starts with the downward movement of a subset of cells at the atrial side of the AVC (brown and red). These cells touch the opposite side of the AVC (E,E′), and their downward movement transforms into a sideward movement (arrows), which brings additional cells in contact with each other (F,F′). Note that for a better view of the valve leaflets, ventral cells covering the AVC were removed in D-F, but can be seen in D′-F′ (asterisk). Cells on the abluminal side are false colored in blue (D-F′). Insets show cartoons of the AVC. A, atrium; I, inferior AVC; S, superior AVC; V, ventricle. Scale bars: 40 μm.

Fig. 5. Notch and Wnt/β-catenin signaling reporters exhibit different expression patterns in the forming cardiac valve and their activity in endocardial cells is dependent on cardiac contraction and/or blood flow. Sagittal planes of *Tg(Tp1:VenusPEST);Tg(Tp1:mCherry-CAAX)* hearts at 70 (A) and 75 (B) hpf. A magnification of the forming valve at 75 hpf is shown in B, inset; single channels are shown in B′ and B″. The expression of both VenusPEST and mCherry-CAAX is driven by the Notch signaling-responsive element *Tp1*. At 75 hpf, in contrast to the mCherry-CAAX signal, which can be detected in both the ventricle and AVC (A,B,B′), the VenusPEST signal is only detectable in a subset of AVC cells lining the lumen (B,B″). At 70 hpf, the VenusPEST signal could also be detected in cells located at the border between the ventricle and AVC (A). (C,D) Sagittal plane of a 75 hpf *Tg(fli1:Gal4db-TΔC-2A-mC);Tg(UAS:EGFP);Tg(fli1:Myr-mCherry)* heart. In contrast to the Notch reporter, the Wnt/β-catenin reporter is mainly expressed on the abluminal side of the valve (arrows). (E) Quantification of the number of AVC endocardial cells expressing VenusPEST of the Notch reporter or EGFP of the Wnt/β-catenin reporter. Data are mean±s.d. of 14±2 VenusPEST^{+} cells (*n*=7 larvae) and 12±2 Wnt/β-catenin^{+} cells (*n*=14 larvae). (F-I) 75 hpf *tnnt2a* morphant hearts (G,I) and hearts of control injected larvae (F,H). Sagittal plane of *Tg(kdrl:ras-mCherry);Tg(Tp1:VenusPEST) tnnt2a* morphant heart shows that *Tp1*:VenusPEST^{+} cells observed in controls (F) are not detectable in non-beating hearts (G). Similarly, the *TCF*:EGFP signal in endocardial cells located at the AVC of control hearts (H, arrow) is downregulated in *Tg(7xTCF-Xla.Siam:EGFP) tnnt2a* morphants (I). A, atrium; V, ventricle. Scale bars: 20 μm.

providing better temporal resolution of Notch activity. At 70 hpf, VenusPEST^{+} cells can be detected in a subset of ventricular cells located at the junction between the ventricle and AVC, as well as at the luminal side of the valve (Fig. 5A). However, VenusPEST^{+} cells were hardly detectable at the abluminal side of the valve. At 75 hpf, the expression of VenusPEST becomes downregulated in the

DEVELOPMENT

ventricular cells, and we counted 14±2 VenusPEST^{+} cells (*n*=7 larvae) that were primarily located at the luminal side of the valve (Fig. 5B,E). In addition, we observed 1-2 VenusPEST^{+} cells that were located at the margin of the forming valve and at its abluminal side. Owing to the peripheral localization of these Notch reporter-positive ALCs, we speculate that they are located at a transitional area between the luminal and abluminal sides of the valve (Fig. S3).

In contrast to Venus, the mCherry-CAAX is not fused to a destabilizing domain and thus its half-life is longer. The *Tp1:*mCherry-CAAX signal can also be detected in ALCs and ventricular cells. Since *notch1b* expression is known to be initially present throughout the endocardium and then becomes restricted during cardiac valve formation (Walsh and Stainier, 2001), we assume that the more stable *Tp1:*mCherry-CAAX signal recapitulates this earlier Notch activity.

Notch signaling activity appears to be much stronger in LCs than in ALCs. However, considering that Notch is required to promote cell migration into the cardiac jelly (Timmerman et al., 2004), we had expected the opposite. Therefore, we investigated whether a similar activation pattern was observable for another signaling pathway also known to facilitate cell migration into the cardiac jelly. For this purpose, we imaged 75 hpf hearts of triple transgenic larvae expressing an endocardial-specific Wnt/β-catenin signaling reporter [*Tg(fli1:Gal4db-TΔC-2A-mC);Tg(UAS:EGFP);Tg(fli1:Myr-mCherry)*] (Asakawa et al., 2008; Kashiwada et al., 2015). In contrast to the Notch reporter data, we could detect Wnt/β-catenin reporter activity in 12±2 cells (*n*=14 larvae) primarily located at the abluminal side of the valve (Fig. 5C-E). Collectively, our observations that reporters for Notch and Wnt/β-catenin signaling are primarily expressed in LCs and ALCs, respectively, show that these two sets of cells are molecularly distinct from each other.

Notch and Wnt/β-catenin signaling in endocardial cells are influenced by cardiac contraction and/or blood flow

Since we found that the Notch and Wnt/β-catenin signaling reporters exhibit different activity patterns in the forming valve and since cardiac valve formation is affected by flow and contractility (Auman et al., 2007; Vermot et al., 2009; Kalogirou et al., 2014), we investigated how the lack of contractility/blood flow affected the activity of these reporters specifically in endocardial cells. We inhibited the heartbeat by injecting *tnnt2a* morpholinos (Sehnert et al., 2002) into one-cell stage Notch [*Tg(Tp1:VenusPEST)*] or Wnt/β-catenin [*Tg(7xTCF-Xla.Siam:EGFP)*] reporter lines. After these injections, the signal of the Notch reporter was no longer detectable in endocardial cells at 75 hpf (*n*=7 larvae) (Fig. 5F,G) in agreement with a recent report (Samsa et al., 2015). Similarly, the strong signal of the Wnt/β-catenin signaling reporter in AVC endocardial cells was downregulated in *tnnt2a* morphants (*n*=8 larvae) (Fig. 5H,I). Collectively, these data indicate that blood flow and/or cardiac contraction modulates the activity of both Notch and Wnt signaling reporters.

Wnt/β-catenin signaling regulates multiple processes influencing cardiac valve formation

We found that Wnt/β-catenin signaling was active only in a subset of cells comprising the immature valve. To examine the effect of disturbed Wnt/β-catenin signaling on cardiac valve formation at the individual cell level, we revisited the *apc* mutant phenotype. *apc* mutants have been described to exhibit enlarged endocardial cushions due to constitutively active Wnt/β-catenin signaling (Hurlstone et al., 2003). We acquired three-dimensional stacks of wild-type and mutant hearts. At all time points examined, *apc*

mutant hearts show a looping defect and a round AVC (*n*=14 embryos) (Fig. 6B′,D′,F′). By contrast, wild-type siblings have an elliptical AVC (Fig. 6A′,C′,E′). At around 60 hpf, the ALCs form a relatively thick valvular structure in *apc* mutants compared with the thin immature valve leaflet in wild-type siblings (*n*=6 embryos) (Fig. 6C-D′). Moreover, the number of endocardial cells that appear to have a cone-shaped nucleus, which might be indicative of cell migration (Friedl et al., 2011; Kim et al., 2014), seems to be increased in *apc* mutants (Fig. 6D″). These cells are predominantly located at the junction between the ventricle and AVC. In wild-type siblings, only one to two cells with a cone-shaped nucleus are detected (Fig. 6C″). However, the restriction of the enlarged valvular structure to the superior AVC appears to correlate with cardiac deterioration in *apc* mutants. As cardiac deterioration progresses, the enlarged valvular structures fall apart (Fig. 6E-F′), and they appear to be replaced by a profuse cell layer surrounding the AVC. However, the number of ALCs is still much higher in *apc* mutants. On average, we observed 20±5 ALCs in *apc* mutants (*n*=8 embryos) versus 10±3 ALCs in wild types (*n*=20 embryos) at 70 hpf (Fig. 2D). Thus, since the number of cone-shaped nuclei in *apc* mutants is increased, we propose that constitutively active Wnt/β-catenin signaling not only leads to increased cell proliferation, as was previously reported (Hurlstone et al., 2003), but also to increased endocardial cell movement towards the AVC cardiac jelly.

DISCUSSION

In this study, we examined the detailed three-dimensional composition of the immature cardiac valve in zebrafish and observed complex cellular rearrangements underlying the formation of this structure. We found that the immature valve is composed of two different sets of cells, which are molecularly distinct from each other and originate from the atrium or ventricle.

In previous reports, it has been suggested that the heart valves in zebrafish embryos are formed directly by an invagination process and not, as in mammals, from mesenchymal endocardial cushions. Although it is clearly recognizable in single confocal planes that endocardial cells remain in a sheet while forming the immature valve leaflets (Scherz et al., 2008), our detailed study indicates that this invaginating sheet is actually composed of two different sets of cells: the LCs and ALCs. LCs and ALCs exhibit differences in (1) signaling: Notch signaling is highly active in LCs and Wnt/β-catenin signaling is active in ALCs; and (2) origin: LCs and ALCs originate from the atrium and ventricle, respectively. As the immature cardiac valve in zebrafish is composed of two distinct cellular structures at its luminal and abluminal sides, we speculate that it exhibits a similar organization to the mesenchymal endocardial cushion in amniotes, which is also composed of two distinct cellular structures: a cushion mesenchyme and an underlying endocardial layer. This observation might indicate a close evolutionary relationship between the immature valve in zebrafish and endocardial cushions in amniotes. However, to what extent the ALCs in zebrafish adopt a mesenchymal state needs to be investigated.

During cardiac valve development in zebrafish, the number of endocardial cells located at the abluminal side of the immature valve increases. Similarly, within the cushion mesenchyme in amniotes, cell numbers also rise over time. This increase has been reported to be due to increased cell proliferation (Markwald et al., 1977). Similarly, endocardial cells of the forming valve in zebrafish were found to be positive for the proliferating cell nuclear antigen (PCNA) (Hurlstone et al., 2003). However, while we employed transgenic lines showing mosaic expression in the endocardium, an
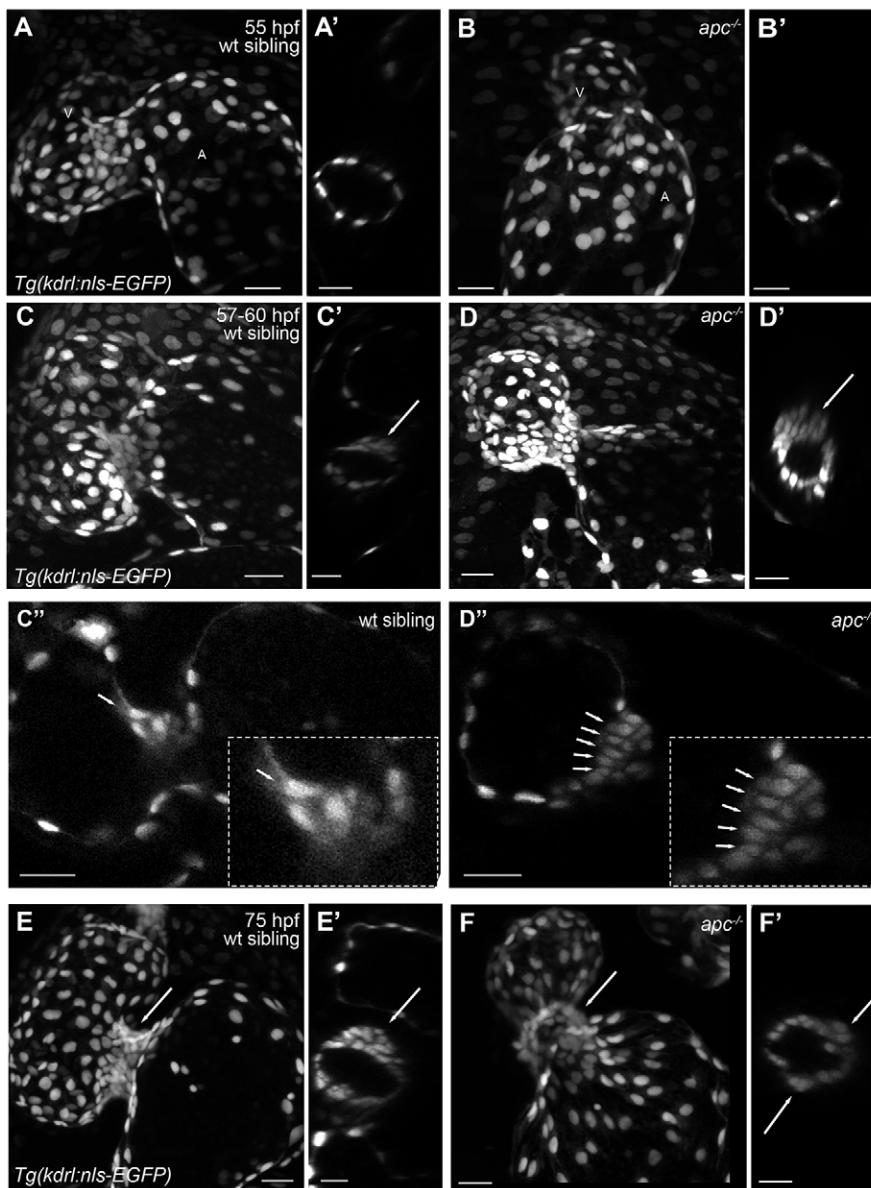
Fig. 6. *apc* mutants exhibit a disorganized accumulation of cells at the AVC. Maximum projection images of *Tg(kdrl:nls-EGFP) apc* mutant (B,D,F) and wild-type sibling (A,C,E) hearts at 55 (A,B), 60 (C,D) and 75 (E,F) hpf. Compared with the wild-type sibling hearts, the *apc* mutant hearts appear elongated (A-D). (C″,D″) Sagittal planes of 60 hpf wild-type sibling and *apc* mutant hearts, respectively. Insets in C″ and D″ show a magnification of the immature valve. At around 60 hpf, the valvular structures appear enlarged in *apc* mutants and more cells exhibit a cone-shaped nucleus (C″,D″, arrows). Note that this valve phenotype appears to depend on the overall phenotype of the heart; as the heart deteriorates the valvular structures at the AVC seem to dissolve. At 75 hpf, the distinctly structured immature valve leaflet in wild-type siblings (E,E′) is replaced by a disorganized accumulation of cells at the AVC of *apc* mutants (F,F′). Transverse planes through the AVC of *apc* mutants (A′-F′) show that these animals exhibit a more circular shaped AVC (B′,D′,F′), instead of the elliptically shaped AVCs seen in wild-type siblings (A′,C′,E′). Cells at the abluminal side of the valve appear to be distributed all around the AVC in *apc* mutants (F′, arrows) and are not restricted to the superior AVC as in wild-type siblings (E′, arrow). A, atrium; V, ventricle. Scale bars: 20 µm.

increase over time in the number of different fluorescent cells comprising the immature valve could not be observed, suggesting that proliferation of LCs and ALCs is not the driving force for the growth of the immature valve leaflet in zebrafish. Instead, we found that cell movements from the chamber endocardium towards the AVC contribute to the formation of the valvular structures. Cells of the immature valve that were found to be positive for PCNA in other studies could, at least in part, be explained by endocardial cells that proliferate before they localized within the immature valve leaflet.

To examine the localization of Wnt/β-catenin signaling activity, we employed various Wnt/β-catenin reporter lines that differ in their expression pattern. While the clear expression of the *Tg(fli1:Gal4db-TΔC-2A-mC);Tg(UAS:GFP)* line could mainly be observed in ALCs, weak expression of the *Tg(7xTCF-Xla.Siam:EGFP)* line could also be observed in LCs. *Tg(7xTCF-Xla.Siam:*nls-mCherry*)* expression, however, was present in both LCs and ALCs. The difference in the activities of these three reporters could be due to the *TCF-Xla.Siam* promoter, which appears to drive strong expression, in addition to an increase

of the signal intensity caused by the concentration of mCherry within the nucleus instead of its distribution throughout the cytosol. This observation may indicate that LCs are also positive for the *Tg(fli1:Gal4db-TΔC-2A-mC);Tg(UAS:GFP)* endothelial Wnt/β-catenin reporter, but at much lower levels than ALCs. Accordingly, Wnt/β-catenin signaling activity in the LCs was also detectable using the *Tg(top:GFP)* line (Hurlstone et al., 2003). This line expresses a destabilized version of GFP and has been reported to be a very weak reporter (Moro et al., 2012). Therefore, in order to increase detection, Hurlstone et al. (2003) performed immunostaining for GFP. This protocol might enhance the signal to an extent that the very low Wnt/β-catenin signaling activity of LCs can also be detected. However, to evaluate the dynamic regulation of Wnt/β-catenin signaling, the lower expression levels of the T*g(7xTCF-Xla.Siam: EGFP)* and *Tg(fli1:Gal4db-TΔC-2A-mC);Tg(UAS:GFP)* lines should make them more sensitive reporters.

Why is Wnt/β-catenin signaling strongly upregulated in ALCs? Wnt/β-catenin activity could also be observed in the mesenchymal endocardial cushions in mice and in AV explants from amniotes. In

comparison to zebrafish, these organisms have a smaller number of endocardial cells that are positive for Wnt/β-catenin activity. Thus, it has been assumed that Wnt/β-catenin signaling is essential for an early/intermediate step during the epithelial to mesenchymal transition (EMT) (Liebner et al., 2004). However, this step might be extended in zebrafish, because all ALCs appear to be positive for the Wnt/β-catenin reporter and, thus, this observation could mean that ALCs undergo a partial, instead of a complete EMT.

The requirement of Wnt/β-catenin signaling for endocardial cell migration towards the abluminal side of the immature valve is also supported by our observation that an increased number of endocardial cells appear to exhibit a cone-shaped nucleus in *apc* mutants. These cone-shaped nuclei could indicate migratory activity (Friedl et al., 2011; Kim et al., 2014), which could, in addition to an increased cell proliferation rate (Hurlstone et al., 2003), cause the enlarged cushions observable in *apc* mutants. The enlarged valvular structures in *apc* mutants (Hurlstone et al., 2003), as well as the lack of endocardial cushions in mice deficient for β-catenin support the role for Wnt/β-catenin signaling in mediating EMT (Liebner et al., 2004). However, Wnt/β-catenin signaling might mediate EMT by increasing cell motility or cell invasion.

During cardiac valve development in zebrafish, *notch1b* is expressed throughout the endocardium at 24 hpf and then becomes restricted to the AVC at ~45 hpf (Walsh and Stainier, 2001). In our studies using a Notch signaling reporter, we observed a similar restriction of Notch signaling to the AVC, suggesting that Notch signaling is involved in cardiac valve formation. Indeed, mice deficient for Notch1, or the Notch effector RBPJκ, lack endocardial cushion cells (Timmerman et al., 2004). Accordingly, injections of the Notch intracellular domain (N1ICD), which leads to constitutively active Notch signaling, causes valve hyperplasia in zebrafish (Timmerman et al., 2004). In addition, the disruption of Notch signaling causes the abnormal maintenance of cell adhesion proteins and keeps endocardial cells at the AVC in close association (Timmerman et al., 2004), further supporting a role for Notch signaling in facilitating EMT and allowing endocardial cells to migrate and contribute to the formation of the immature valve.

However, why did we observe a restriction of the destabilized Notch reporter not only to the AVC, but also to LCs, to that part of the immature valve where endocardial cells actually appear strongly associated with each other and only show low levels of cell movements? In contrast to the ubiquitous overexpression of *N1ICD* mRNA, which might activate additional signals within the myocardium (Timmerman et al., 2004), overexpression of *N1ICD* specifically in endothelial cells inhibits valve formation in zebrafish (Beis et al., 2005). Furthermore, immunostaining in mice using an antibody against N1ICD showed strong Notch activity in cells at the AVC that are about to undergo EMT, whereas mesenchymal cushion cells were negative (Del Monte et al., 2007). Moreover, it has been observed that Notch1 is sufficient to activate a promesenchymal gene expression program in amniotes (Luna-Zurita et al., 2010). Taken together, these results might indicate that Notch signaling is initially required to activate a gene expression program to facilitate valve formation, but that it needs to be downregulated to allow the subsequent cellular rearrangements underlying valve formation. These observations may also provide additional evidence that the abluminal side of the forming valves in zebrafish resembles endocardial cushions in amniotes.

In our experiments, we examined *tnnt2a* morphants to investigate the influence of cardiac contraction and/or blood flow on Notch and Wnt/β-catenin signaling and found that both pathways were altered in the absence of a heartbeat. In *tnnt2a* morphants, Wnt/β-catenin

signaling was downregulated in the endocardium, indicating that contraction and/or blood flow are essential for Wnt/β-catenin signaling in these cells. Similarly, Notch signaling could not be detected in endocardial cells in *tnnt2a* morphants at 75 hpf. These observations are in line with previous reports showing that *notch1b* expression is undetectable in *tnnt2a* morphants at 48-50 hpf (Samsa et al., 2015) and is also downregulated in *gata2* morphants, which have a lower blood viscosity (Vermot et al., 2009). Taken together, these results indicate that both Notch and Wnt/β-catenin signaling depend on cardiac contraction and/or blood flow.

In summary, our findings in zebrafish illustrate the complex cellular rearrangements during cardiac valve development *in vivo* and will help future analyses of the signaling pathways involved in this process at the single cell level.

MATERIALS AND METHODS
Zebrafish husbandry
Adult and embryonic zebrafish were raised and maintained under standard laboratory conditions (Westerfield, 1993) according to institutional guidelines. The following transgenic and mutant lines were used: *Tg(kdrl:EGFP)^{s843}* (Jin et al., 2005), *Tg(7xTCF-Xla.Siam:nls-mCherry)^{ia5}* (Moro et al., 2012), *Tg(kdrl:nls-EGFP)^{zf109}* (Blum et al., 2008), *Tg(kdrl:ras-mCherry)^{s896}* (Chi et al., 2008), *Tg(UAS:Kaede)^{rk8Tg}* (Hatta et al., 2006), *Tg(fli1a:Gal4FF)^{ubs4}* (Zygmunt et al., 2011), *Tg(UAS:Brainbow)^{s1997t}* (Robles et al., 2013), *Tg(UAS:GFP)^{nkuasgfp1a}* (Asakawa et al., 2008), *Tg(TP1:VenusPEST)^{s940}* (Ninov et al., 2012), *apc^{hu745/+}* (Hurlstone et al., 2003), *Tg(fli1:Gal4db-TΔC-2A-mC)^{ncv15}* and *Tg(fli1:Myr-mCherry)^{ncv1}* (Kashiwada et al., 2015).

Generation of transgenic lines
Tg(Tp1bglob:mCherry-CAAX)^{s1015} [abbreviated as *Tg(TP1:VenusPEST)*] and *Tg(Tp1bglob:LIFEACT-mCherry)^{s732}* [*Tg(TP1:LIFEACT-mCherry)*], were generated using the pT2KXIGΔin backbone (Urasaki et al., 2006).

TgBAC(nfatc1:GAl4ff)^{mu286} was generated by recombining the *GAl4ff* sequence (Bussmann and Schulte-Merker, 2011) into the genomic region of the *nfatc1* locus in the bacterial artificial chromosome (BAC) clone CH211-198C22 (BACPAC Resources Center). All recombination steps were performed as described (Bussmann and Schulte-Merker, 2011). The primers to generate the targeting PCR products of iTol2_Amp cassette were described previously (Bussmann and Schulte-Merker, 2011). The following primers were used to generate the targeting PCR products of Gal4_Kan cassette: nfatc1_HA1_Gal4_fw, 5′-GTTTTGGAAAAGTG-CGTTGAACTTGCTGTGAGTTCTGTCTACACTTCGCAACCATGAA-GCTACTGTCTTCTATCGAAC-3′ and nfatc1_HA2_kanR_rev, 5′-GAGACAGTAGATGCATTTAATCAGAATACGTTACCTTCCTCTGC-GATTTTCAGAAGAACTCGTCAAGAAGGCG-3′. Transgenics were generated in AB or TL strains using the tol-2 system (Kawakami et al., 2004).

Morpholino and mRNA injections
To generate *tnnt2a* and *apc* morphants, 0.25 ng *tnnt2a* morpholino (5′-CATGTTTGCTCTGATCTGACACGCA-3′) or 4 ng *apc* morpholino (5′-TAGCATACTCTACCTGTGCTCTTCG-3′) was injected into one-cell stage embryos subsequently raised at 28°C and imaged at 75 hpf. To trigger the recombination in *Tg(UAS:Brainbow)* fish, we injected 0.15 ng of *Cre* mRNA into one-cell stage embryos.

Confocal microscopy
For *in vivo* analyses of cardiac valve formation at cellular resolution, the embryos were mounted in 1.5% low-melting agarose containing 0.2% tricaine. The high concentration of tricaine stopped the heartbeat and then high-resolution confocal images were obtained. The images were acquired using a Zeiss LSM 780 confocal microscope. If the embryo was to be imaged again at a later time point, it was dismounted and transferred to fresh egg water. In this way, the tricaine was immediately washed out and the heart started beating again until the embryo was re-mounted for the next

imaging time point. During this entire procedure, the heartbeat was never stopped for longer than 25 min.

For imaging beating hearts, embryos were mounted in 1% low-melting agarose containing 0.015% tricaine on a glass-bottom dish. The movies were acquired with an inverted Zeiss Cell Observer SD microscope, equipped with a Yokogawa CSU-X1 spinning disk and a dual-channel (ORCA-Flash4.0V2 Digital CMOS camera) system at a minimum acquisition rate of 100 frames per second. The acquired dataset was post-acquisitionally aligned in MATLAB software using a previously published algorithm (Liebling et al., 2005, 2006; Ohn et al., 2009).

The fluorophore Kaede was photoconverted by a 1-μm-step scan through the embryonic heart using the 405 nm diode laser of the LSM 780 with an open pinhole. Then, photoconversion was verified by checking the change of the emission wavelength from 518 to 582 nm.

Image processing

The acquired 3D dataset was processed and volume rendered using Imaris (Bitplane). Maximum projections of z-stack were created with Fiji. In addition, Fiji was employed for processing single-plane images and Imaris was used for cell counting. Furthermore, apart from Fig. 5, a gamma correction value between 0.7 and 1.3 was applied.

References

Ahuja, S., Dogra, D., Stainier, D. Y. and Reischauer, S. (2016). Id4 functions downstream of Bmp signaling to restrict TCF function in endocardial cells during atrioventricular valve development. *Dev. Biol.* **412**, 71-82.

Armstrong, E. J. and Bischoff, J. (2004). Heart valve development: endothelial cell signaling and differentiation. *Circ. Res.* **95**, 459-470.

Asakawa, K., Suster, M. L., Mizusawa, K., Nagayoshi, S., Kotani, T., Urasaki, A., Kishimoto, Y., Hibi, M. and Kawakami, K. (2008). Genetic dissection of neural circuits by Tol2 transposon-mediated Gal4 gene and enhancer trapping in zebrafish. *Proc. Natl. Acad. Sci. USA* **105**, 1255-1260.

Auman, H. J., Coleman, H., Riley, H. E., Olale, F., Tsai, H.-J. and Yelon, D. (2007). Functional modulation of cardiac form through regionally confined cell shape changes. *PLoS Biol.* **5**, e53.

Bartman, T., Walsh, E. C., Wen, K.-K., McKane, M., Ren, J., Alexander, J., Rubenstein, P. A. and Stainier, D. Y. R. (2004). Early myocardial function affects endocardial cushion development in zebrafish. *PLoS Biol.* **2**, e129.

Beis, D. and Stainier, D. Y. R. (2006). In vivo cell biology: following the zebrafish trend. *Trends Cell Biol.* **16**, 105-112.

Beis, D., Bartman, T., Jin, S.-W., Scott, I. C., D'amico, L. A., Ober, E. A., Verkade, H., Frantsve, J., Field, H. A., Wehman, A. et al. (2005). Genetic and cellular analyses of zebrafish atrioventricular cushion and valve development. *Development* **132**, 4193-4204.

Blum, Y., Belting, H.-G., Ellertsdottir, E., Herwig, L., Lüders, F. and Affolter, M. (2008). Complex cell rearrangements during intersegmental vessel sprouting and vessel fusion in the zebrafish embryo. *Dev. Biol.* **316**, 312-322.

Brown, C. B., Boyer, A. S., Runyan, R. B. and Barnett, J. V. (1999). Requirement of type III TGF-beta receptor for endocardial cell transformation in the heart. *Science* **283**, 2080-2082.

Bussmann, J. and Schulte-Merker, S. (2011). Rapid BAC selection for tol2-mediated transgenesis in zebrafish. *Development* **138**, 4327-4332.

Camenisch, T. D., Schroeder, J. A., Bradley, J., Klewer, S. E. and McDonald, J. A. (2002). Heart-valve mesenchyme formation is dependent on hyaluronan-augmented activation of ErbB2-ErbB3 receptors. *Nat. Med.* **8**, 850-855.

Chang, C.-P., Neilson, J. R., Bayle, J. H., Gestwicki, J. E., Kuo, A., Stankunas, K., Graef, I. A. and Crabtree, G. R. (2004). A field of myocardial-endocardial NFAT signaling underlies heart valve morphogenesis. *Cell* **118**, 649-663.

Chi, N. C., Shaw, R. M., De Val, S., Kang, G., Jan, L. Y., Black, B. L. and Stainier, D. Y. R. (2008). Foxn4 directly regulates tbx2b expression and atrioventricular canal formation. *Genes Dev.* **22**, 734-739.

de la Pompa, J. L., Timmerman, L. A., Takimoto, H., Yoshida, H., Elia, A. J., Samper, E., Potter, J., Wakeham, A., Marengere, L. et al. (1998). Role of the NF-ATc transcription factor in morphogenesis of cardiac valves and septum. *Nature* **392**, 182-186.

Del Monte, G., Grego-Bessa, J., González-Rajal, A., Bolós, V. and de la Pompa, J. L. (2007). Monitoring Notch1 activity in development: evidence for a feedback regulatory loop. *Dev. Dyn.* **236**, 2594-2614.

Forouhar, A. S., Liebling, M., Hickerson, A., Nasiraei-Moghaddam, A., Tsai, H.-J., Hove, J. R., Fraser, S. E., Dickinson, M. E. and Gharib, M. (2006). The embryonic vertebrate heart tube is a dynamic suction pump. *Science* **312**, 751-753.

Friedl, P., Wolf, K. and Lammerding, J. (2011). Nuclear mechanics during cell migration. *Curr. Opin. Cell Biol.* **23**, 55-64.

Gitler, A. D., Lu, M. M., Jiang, Y. Q., Epstein, J. A. and Gruber, P. J. (2003). Molecular markers of cardiac endocardial cushion development. *Dev. Dyn.* **228**, 643-650.

Goishi, K., Lee, P., Davidson, A. J., Nishi, E., Zon, L. I. and Klagsbrun, M. (2003). Inhibition of zebrafish epidermal growth factor receptor activity results in cardiovascular defects. *Mech. Dev.* **120**, 811-822.

Hatta, K., Tsujii, H. and Omura, T. (2006). Cell tracking using a photoconvertible fluorescent protein. *Nat. Protoc.* **1**, 960-967.

Hurlstone, A. F. L., Haramis, A.-P. G., Wienholds, E., Begthel, H., Korving, J., Van Eeden, F., Cuppen, E., Zivkovic, D., Plasterk, R. H. A. and Clevers, H. (2003). The Wnt/beta-catenin pathway regulates cardiac valve formation. *Nature* **425**, 633-637.

Iwamoto, R., Yamazaki, S., Asakura, M., Takashima, S., Hasuwa, H., Miyado, K., Adachi, S., Kitakaze, M., Hashimoto, K., Raab, G. et al. (2003). Heparin-binding EGF-like growth factor and ErbB signaling is essential for heart function. *Proc. Natl. Acad. Sci. USA* **100**, 3221-3226.

Jin, S.-W., Beis, D., Mitchell, T., Chen, J.-N. and Stainier, D. Y. R. (2005). Cellular and molecular analyses of vascular tube and lumen formation in zebrafish. *Development* **132**, 5199-5209.

Kalogirou, S., Malissovas, N., Moro, E., Argenton, F., Stainier, D. Y. R. and Beis, D. (2014). Intracardiac flow dynamics regulate atrioventricular valve morphogenesis. *Cardiovasc. Res.* **104**, 49-60.

Kashiwada, T., Fukuhara, S., Terai, K., Tanaka, T., Wakayama, Y., Ando, K., Nakajima, H., Fukui, H., Yuge, S., Saito, Y. et al. (2015). beta-Catenin-dependent transcription is central to Bmp-mediated formation of venous vessels. *Development* **142**, 497-509.

Kawakami, K., Takeda, H., Kawakami, N., Kobayashi, M., Matsuda, N. and Mishina, M. (2004). A transposon-mediated gene trap approach identifies developmentally regulated genes in zebrafish. *Dev. Cell* **7**, 133-144.

Kim, R. Y., Robertson, E. J. and Solloway, M. J. (2001). Bmp6 and Bmp7 are required for cushion formation and septation in the developing mouse heart. *Dev. Biol.* **235**, 449-466.

Kim, D.-H., Cho, S. and Wirtz, D. (2014). Tight coupling between nucleus and cell migration through the perinuclear actin cap. *J. Cell Sci.* **127**, 2528-2541.

Liebling, M., Forouhar, A. S., Gharib, M., Fraser, S. E. and Dickinson, M. E. (2005). Four-dimensional cardiac imaging in living embryos via postacquisition synchronization of nongated slice sequences. *J. Biomed. Opt.* **10**, 054001.

Liebling, M., Forouhar, A. S., Wolleschensky, R., Zimmermann, B., Ankerhold, R., Fraser, S. E., Gharib, M. and Dickinson, M. E. (2006). Rapid three-dimensional imaging and analysis of the beating embryonic heart reveals functional changes during development. *Dev. Dyn.* **235**, 2940-2948.

Liebner, S., Cattelino, A., Gallini, R., Rudini, N., Iurlaro, M., Piccolo, S. and Dejana, E. (2004). Beta-catenin is required for endothelial-mesenchymal transformation during heart cushion development in the mouse. *J. Cell Biol.* **166**, 359-367.

Lloyd-Jones, D., Adams, R. J., Brown, T. M., Carnethon, M., Dai, S., De Simone, G., Ferguson, T. B., Ford, E., Furie, K., Gillespie, C. et al. (2010). Heart disease and stroke statistics–2010 update: a report from the American Heart Association. *Circulation* **121**, e46-e215.

Luna-Zurita, L., Prados, B., Grego-Bessa, J., Luxán, G., Del Monte, G., Benguría, A., Adams, R. H., Pérez-Pomares, J. M. and de la Pompa, J. L. (2010). Integration of a Notch-dependent mesenchymal gene program and Bmp2-

DEVELOPMENT

driven cell invasiveness regulates murine cardiac valve formation. *J. Clin. Invest.* **120**, 3493-3507.

Ma, L., LU, M.-F., Schwartz, R. J. and Martin, J. F. (2005). Bmp2 is essential for cardiac cushion epithelial-mesenchymal transition and myocardial patterning. *Development* **132**, 5601-5611.

Markwald, R. R., Fitzharris, T. P. and Manasek, F. J. (1977). Structural development of endocardial cushions. *Am. J. Anat* **148**, 85-119.

Moro, E., Ozhan-Kizil, G., Mongera, A., Beis, D., Wierzbicki, C., Young, R. M., Bournele, D., Domenichini, A., Valdivia, L. E., Lum, L. et al. (2012). In vivo Wnt signaling tracing through a transgenic biosensor fish reveals novel activity domains. *Dev. Biol.* **366**, 327-340.

Ninov, N., Borius, M. and Stainier, D. Y. R. (2012). Different levels of Notch signaling regulate quiescence, renewal and differentiation in pancreatic endocrine progenitors. *Development* **139**, 1557-1567.

Ohn, J., Tsai, H.-J. and Liebling, M. (2009). Joint dynamic imaging of morphogenesis and function in the developing heart. *Organogenesis* **5**, 248-255.

Ranger, A. M., Grusby, M. J., Hodge, M. R., Gravallese, E. M., de la Brousse, F. C., Hoey, T., Mickanin, C., Baldwin, H. S. and Glimcher, L. H. (1998). The transcription factor NF-ATc is essential for cardiac valve formation. *Nature* **392**, 186-190.

Rivera-Feliciano, J., Lee, K.-H., Kong, S. W., Rajagopal, S., Ma, Q., Springer, Z., Izumo, S., Tabin, C. J. and Pu, W. T. (2006). Development of heart valves requires Gata4 expression in endothelial-derived cells. *Development* **133**, 3607-3618.

Robles, E., Filosa, A. and Baier, H. (2013). Precise lamination of retinal axons generates multiple parallel input pathways in the tectum. *J. Neurosci.* **33**, 5027-5039.

Samsa, L. A., Givens, C., Tzima, E., Stainier, D. Y. R., Qian, L. and Liu, J. (2015). Cardiac contraction activates endocardial Notch signaling to modulate chamber maturation in zebrafish. *Development* **142**, 4080-4091.

Scherz, P. J., Huisken, J., Sahai-Hernandez, P. and Stainier, D. Y. R. (2008). High-speed imaging of developing heart valves reveals interplay of morphogenesis and function. *Development* **135**, 1179-1187.

Sehnert, A. J., Huq, A., Weinstein, B. M., Walker, C., Fishman, M. and Stainier, D. Y. R. (2002). Cardiac troponin T is essential in sarcomere assembly and cardiac contractility. *Nat. Genet.* **31**, 106-110.

Stainier, D. Y. (2001). Zebrafish genetics and vertebrate heart formation. *Nat. Rev. Genet.* **2**, 39-48.

Timmerman, L. A., Grego-Bessa, J., Raya, A., Bertrán, E., Pérez-Pomares, J. M., Díez, J., Aranda, S., Palomo, S., Mccormick, F., Izpisua-Belmonte, J. C et al. (2004). Notch promotes epithelial-mesenchymal transition during cardiac development and oncogenic transformation. *Genes Dev.* **18**, 99-115.

Urasaki, A., Morvan, G. and Kawakami, K. (2006). Functional dissection of the Tol2 transposable element identified the minimal cis-sequence and a highly repetitive sequence in the subterminal region essential for transposition. *Genetics* **174**, 639-649.

Vermot, J., Forouhar, A. S., Liebling, M., Wu, D., Plummer, D., Gharib, M. and Fraser, S. E. (2009). Reversing blood flows act through klf2a to ensure normal valvulogenesis in the developing heart. *PLoS Biol.* **7**, e1000246.

Walsh, E. C. and Stainier, D. Y. R. (2001). UDP-glucose dehydrogenase required for cardiac valve formation in zebrafish. *Science* **293**, 1670-1673.

Westerfield, M. (1993). *The Zebrafish Book: A Guide for the Laboratory Use of Zebrafish (Brachydanio rerio)*. Eugene, OR: University of Oregon Press.

Zygmunt, T., Gay, C. M., Blondelle, J., Singh, M. K., Flaherty, K. M., Means, P. C., Herwig, L., Krudewig, A., Belting, H.-G., Affolter, M. et al. (2011). Semaphorin-PlexinD1 signaling limits angiogenic potential via the VEGF decoy receptor sFlt1. *Dev. Cell* **21**, 301-314.